Interconnection Performance Analysis of Single Phase Neural Network Based NPC and CHB Multilevel Inverters for Grid-Connected PV Systems

M. Keddar *‡, M. L. Doumbia*, M. Della Krachai**, K. Belmokhtar*, A.H Midoun**

* Department of Electrical and Computer Engineering, Université du Québec à Trois-Rivières 3351, boul. des Forges, Trois-Rivières (Québec) G9A 5H7, Canada

** Department of Electrical Engineering, University of Science and Technology Mohamed Boudiaf at Oran, El Mnaouar, BP 1505, Bir El Djir 31000, Oran, Algérie.

(mohamed.keddar@uqtr.ca, mamadou.doumbia@uqtr.ca, mohamed.dellakrachai@univ-usto.dz, Karim.belmokhtar@uqtr.ca)

‡ Corresponding author: M. Keddar; email: mohamed.keddar@uqtr.ca, Tel: +1 819 376 5011 ext. 3912

Received: 16.07.2019 Accepted:04.09.2019

Abstract- This paper presents the interconnection performance analysis of single-phase cascaded H-bridge and neutral point clamped multilevel inverters for grid-connected photovoltaic (PV) applications. Interconnection performance analysis of both inverters was investigated using fixed and variable bands hysteresis current control strategies to ensure a lower current's total harmonic distortion (THD). An intelligent control method based on neural networks was introduced to extract maximum power from the PV modules and to achieve optimal operation of the whole system when connected to the utility grid. Control algorithm was implemented in a microcontroller with interrupt routines priority. Both simulation and experimental results are presented to verify the performance of the proposed control methods. In addition, islanding detection capability of the two topologies was investigated.

Keywords: Photovoltaic system, Multilevel Inverter, MPPT, Neural Networks, Hysteresis control.

1. Introduction

In recent years, renewable energy sources (RES) become more and more popular due to their contribution to the total energy consumed in the world and their potential contribution in reducing environmental pollution and greenhouse effect. In this context, microgrids become an attractive solution to enhance the reliability of the electric power system and to electrify isolated sites. The aim is to increase the penetration of Distributed Energy Resources (DER) and ensure the system safety and stability [1]. Recently, many PV systems such as autonomous, grid connected and water pumping applications have been developed. Grid connected photovoltaic systems are an important form of photovoltaic generation [2]. In general, PV systems include two important power parts [3]. The first one is dc-dc converter, generally it is used to extract the maximum power from sources and to protect the input side. The second one is the inverter which controls the power flow, grid synchronization, islanding protection, etc. DC-dc converters are used to increase the extracted energy from PV modules. This achievement can be done using the maximum power point tracker (MPPT). Recently, many algorithms for tracking the maximum power point have been proposed in the literature. They are used to adjust output power considering weather changes [4]. In [5] incremental conductance MPPT method was used. Authors have proposed a cascaded H-bridge multilevel inverter topology with a MPPT controller for each H-bridge to solve the PV mismatch issue. This controller was used to generate the voltage reference for each H-bridge. In [6] a dc–dc converter was used with the perturb and observe method to track the maximum power point (MPP) through the control of the PV voltages. This method is popular and is used in different renewable energy systems such as wind energy systems [7]. To avoid the use of high cost sensors in the MPPT methods, artificial intelligence such as fuzzy logic can be used to control the duty cycle of the boost converter under variable weather conditions [8]; then another converter controls the charge of the battery [9]. Neural networks based methods demonstrate fast convergence response with more accuracy for MPPT control. One of them is Radial Basis Function

Network (RBFN), which is capable of controlling at the same time the non-linearity and time varying condition for grid connected PV systems [10].

Inverter is one of the key components of a grid-connected photovoltaic system for interfacing renewable energy to the grid. Its topology can be current or voltage sources [11]. In last years multilevel inverters have been widely used in power systems. Indeed, a variety of topologies such as diode-clamped, capacitor-clamped and cascaded H-bridge structures have been presented and developed. Multilevel inverters offer a good output waveform, low switching stress and redundancy due to modularity such as in the cascaded H-bridge topology. This topology uses independent sources for each H-bridge module. This makes possible independent voltage control [5,12]. Modularity is also an advantage for this topology of inverters [13]. Neutral point clamped (NPC) multilevel inverters have minimum ripples in the output current and reducing the switching stresses [14,15]. Other topologies of multilevel inverters such as flying-capacitor [16] can be found in the literature. The control of multilevel inverters is more complicated than classical two level inverters. In the literature, many techniques of pulse width modulation (PWM) are proposed for inverters control [10]. These methods are based on voltage and/or current control [17]. In [18] the authors present the direct power control method (DPC) with space vector modulation (SVM). This method gives a rapid dynamic response and overcomes disadvantages such as harmonic reference tracking [19]. In recent years, many hysteresis current control (HCC) methods have been presented in the literature [20-22]. In [20] a comparative analysis of both fixed and adaptive band HCC is given and authors have fixed the issue of variable switching frequency. In [21] a modified multiband hysteresis current controller is used with a cascaded H bridge with modulated vector control to keep the switching frequency constant. This method was used to fix undesired torque and speed ripples of direct torque controlled induction motor drive. There are other HCC methods in the literature, based on fuzzy logic [22] to make the hysteresis band adaptive and to maintain the switching frequency constant. The connection of DER to the grid network needs also islanding protection. Islanding methods are classified as active, passive, hybrid and communication-based methods [23,25]. The passive methods detect the parameters changes (frequency, voltage, etc.) at the point of common coupling (PCC). If the measured value exceeds predefined limits, the DER must be islanded. In this paper we used only the passive methods to detect the islanding phenomena.

Compared with classical two or three levels inverter topologies, multilevel inverters offer a good output waveform and low switching stress. In this paper, two types of grid-connected multilevel inverters (cascaded H-bridge and neutral point clamped) for PV systems are investigated and compared in order to choice the best topology for practical implementation for our feature research test bench. MPPT algorithm based on feed-forward neural networks has been introduced to eliminate the DC-DC converter and the use of expensive sensors. A hysteresis current controller with a fixed and variable band performed the control of the inverters. The system configuration is presented in section II. Section III describes the control strategy. Simulation results using Matlab/Simulink are provided in section IV. Section V gives experimental results of the developed laboratory prototype. The control algorithms were validated for both inverter topologies.

2. System Configuration

An overview of the whole system is depicted in Fig.1. It's composed of photovoltaic generator (PVG), maximum power point tracker (MPPT), multilevel inverter and the control blocks.

2.1. Maximum Power Point Tracking

To increase efficiency of PV systems, it's important to extract maximum power using an MPPT controller. PVG's power depends on two weather parameters, irradiance and temperature. Thus, since both irradiance and temperature are constantly changing, the maximum power point is not fixed. Increasing irradiation gives a proportional increase in maximal power point. But increasing temperature gives a decrease in maximal power point [26].

Fig. 2 and fig.3 show the effects of irradiance and temperature on the PV cell. In literature many MPPT methods have been developed [5,6,26,27,28]. Perturb and observe, incremental conductance and hill climbing are conventional methods. Neural networks, fuzzy logic and genetic algorithms based are mentioned as artificial intelligence methods. Accuracy, complexity of implementation, sensors requirements and costs, convergence speed and popularity of these methods are different. In this paper, artificial intelligence Feed Forward Neural Networks (FFNNet) method is used.

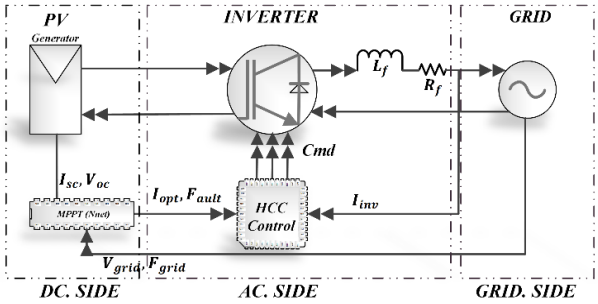

Fig. 1. System Configuration

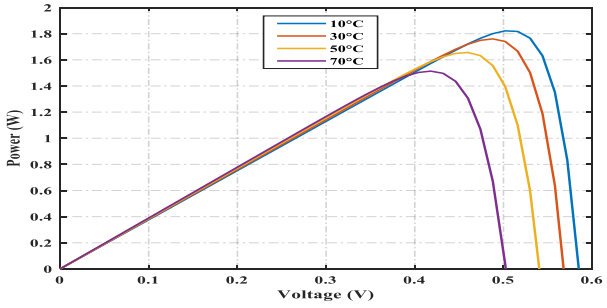

Fig. 2. Temperature effect on the PV cell.

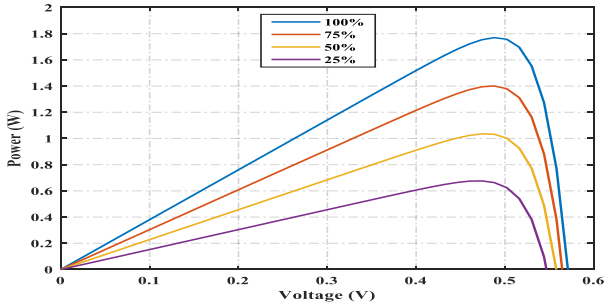

Fig. 3. Irradiance effect on the PV cell.

Fig. 4. shows a general architecture of a neural network which is composed of three layers: input, hidden and output layers. In our case, PV parameters can be used as input variables like open circuit voltage, temperature, irradiance, short circuit current, power, etc. The output variable can be the duty cycle for the PWM converters, the optimum current, voltage or power. In this study, the open circuit voltage (V_{oc}) and short circuit current (I_{sc}) are used as inputs for the input layer, which are proportional to the variation of temperature and irradiance respectively. The optimal current (I_{opt}) is used as output variable of the output layer. of solar irradiation and temperature. These parameters are taken from the V_{oc} and I_{sc} by using the neural network algorithm.

MATLAB neural network toolbox was used for the training of the algorithm with experimental data provided by a weather station located in our laboratory. The parameters of the training process were implemented in a microcontroller to track the MPP and calculate the optimum current I_{opt}.

Then, the calculated I_{opt} is used as a current reference by the multilevel inverters controller in order to operate closer to the maximum power point and to increase the efficiency of the system. Fig. 5 shows the acquired data for one day's measurement. The algorithm computes the I_{opt} every five minutes. The figure shows the short circuit current and the optimum current measurements. The two curves have similar shapes, this confirms the proportional relationship between I_{opt} and I_{sc}.

2.2. Cascaded multilevel inverter

This topology contains two H-bridge inverters connected in series, as illustrated in fig. 6. Each H-bridge is connected to PV panels string. The inverter generates an output voltage of five levels 0, +V/2, +V, –V and –V/2 where V is the summation of V_1 and V_2.

These voltage levels reduce the filter size at the output by reducing the harmonics in the generated current.

Each H-bridge is composed of four power switches, four diodes and one capacitor. Each H-bridge can generate three voltage levels in the output, 0, $+V_1$ and $-V_1$.

The equivalent switching function of the cascaded inverter is given by Eq.(1):

$$V_{inv} = (T_1T_6 - T_2T_5)V_1 + (T_3T_8 - T_4T_7)V_2 \quad (1)$$

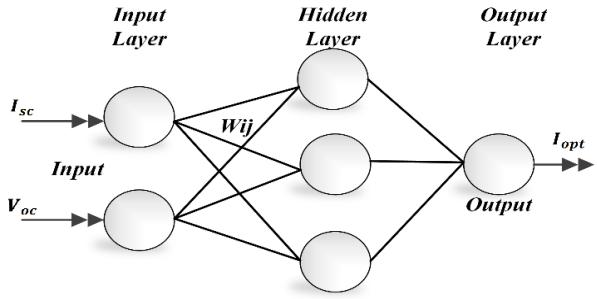

Fig. 4. Neural network architecture.

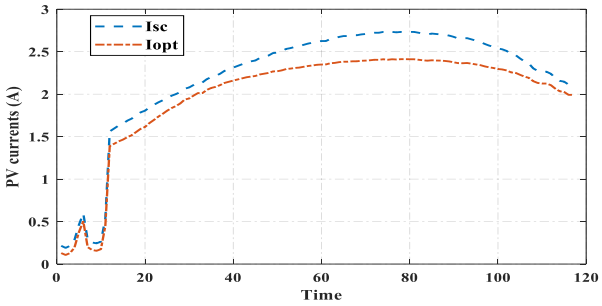

Fig. 5. Results of the developed Neural Network MPP tracker

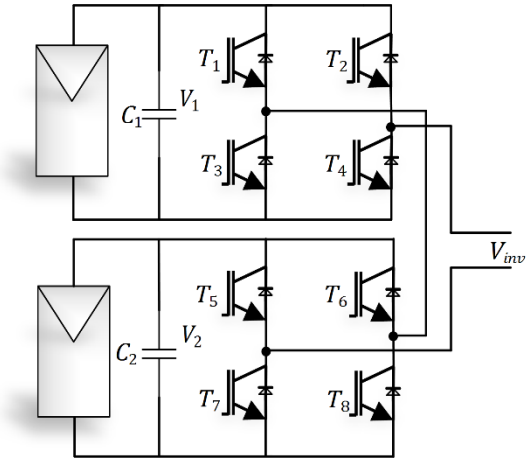

Fig. 6. Cascaded inverter topology

To avoid a short circuit in each leg the power switches T_1, T_3, T_5, T_7 are opposite of T_2, T_4, T_6, and T_8. Table 1 gives the valid state of the power switches and the corresponding voltage. There are eight valid switching states. Two states produce the voltage +V/2, two for -V/2, two for state 0, one for +V and one for –V.

2.3. NPC multilevel inverter

Fig. 7. shows the main circuit of the NPC multilevel inverter. The inverter is composed of six power switches, four in leg a, and two in leg b, two neutral point clamped diodes, and two capacitors. The inverter can generate five output voltage levels.

Table 1. Valid switching states for cascaded multilevel inverter

T_1	T_2	T_5	T_6	V_{inv}
1	0	1	0	V
1	0	0	0	V/2
0	0	1	0	V/2
1	0	0	1	0
0	1	1	0	0
0	1	0	0	-V/2
0	0	0	1	-V/2
0	1	0	1	-V

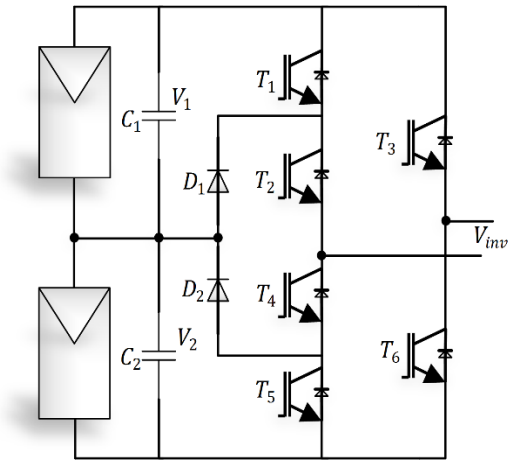

Fig. 7. Topology of the NPC multilevel inverter

Table 2 presents the output voltages and switching states of power switches. These are: 0, V/2, V, -V/2 and –V. Each capacitor has a voltage of V/2 [29].

3. Control strategy

3.1. Hysteresis current controller

The control strategy is based on hysteresis current control (HCC) in order to follow the PV maximal current reference delivered by MPPT algorithm. Two types of HCC, fixed band and variable band, were used. The fixed band method has a low switching frequency with a less power losses compared to the variable band technique and its practical implementation is easy.

Table 2. Valid switching states for neutral point clamped multilevel inverter

T_1	T_2	T_3	T_4	T_5	T_6	V_{inv}
1	1	1	0	0	0	0
1	1	0	0	0	1	V
0	1	1	1	0	0	- V/2
0	1	0	1	0	1	V /2
0	0	1	1	1	0	- V
0	0	0	1	1	1	0

However, the variable band method has a lower THD and it is more complex for implementation. To generate the inverter's switching signals, the control system needs the following information: the utility signal alternation (positive or negative), the operation region and the PWM command, which is based on the comparison between optimal current I_{opt} and the inverter output current. So, control signals are given by Eq. (2) [29].

The error between the two currents is represented by Δi. This error is chosen by the operator; B represents the hysteresis band; the signal K_1 is used to define the positive or negative sign of the grid voltage (V_s), it is derived from the phase-locked loop (PLL).

$$K_1 = \begin{cases} 0 \;\; if \;\; V_s > 0 \\ 1 \;\; if \;\; V_s < 0 \end{cases}$$

$$K_2 = \begin{cases} 0 \;\; if \; \dfrac{-V}{2} < V_s < \dfrac{V}{2} \\ 1 \;\; if \;\; -V < V_s < -\dfrac{V}{2} or \; V > V_s > \dfrac{V}{2} \end{cases} \qquad (2)$$

$$K_3 = \begin{cases} 0 \;\; if \;\; \Delta_i > B \\ 1 \;\; if \;\; \Delta_i < -B \end{cases}$$

K_1 has two states, one when V_s>0 and zero when V_s<0. Signal K_2 is used to determinate zones, it is derived from the comparison of V_s and V_s/2. Two zones are defined, the first zone when V_s is greater than -V/2 and less than V/2, and the second zone when the V_s is less than V, but greater than V/2. V represents the DC link voltage. K_3 represents the comparison between the inverter current I_{inv} and optimal I_{opt}. It is used to keep the inverter output current I_{inv} near the optimal current I_{opt}. Fig. 8 illustrates the control scheme. In this paper fixed hysteresis band (FHB) and variable hysteresis band (VHB) current controllers have been used. The output voltage of the inverter can be given in Eq. (3) [27].

Table 3. summarizes the output voltage values of the two multilevel inverters.

Table 3. Control signals and corresponding voltage.

K_1	K_2	K_3	V_{inv}
0	0	0	0
0	0	1	V_2
0	1	0	V_2
0	1	1	V_1+V_2
1	0	0	$-V_1$
1	0	1	0
1	1	0	$-(V_1+V_2)$
1	1	1	$-V_1$

$$V_s - V_{inv} = L\frac{di}{dt} + Ri \quad (3)$$

And the reference current as Eq. (4):

$$I_{ref} = \sqrt{2} I_{opt} \sin(\omega t) \quad (4)$$

For the FHB, the upper and lower limits are:

Upper band: $I_{up} = I_{ref}(\mathrm{t}) + \Delta \mathrm{i}$ (5)

Lower band: $I_{lw} = I_{ref}(\mathrm{t}) - \Delta \mathrm{i}$ (6)

For the VHB Eq. (7,8):

Upper band: $I_{up} = \left(I_{ref}(\mathrm{t}) + \Delta \mathrm{i}\right) \sin(\omega t)$ (7)

Lower band: $I_{lw} = \left(I_{ref}(\mathrm{t}) - \Delta \mathrm{i}\right) \sin(\omega t)$ (8)

3.2. Algorithm implementation

The inverters switching signals are shown in fig. 8. The control equations can be established using the Karnaugh simplification. This logic control has been implemented inside a programmable logic circuit the GAL22V10.
The relations between control signals and switching signals can be given as:

For the cascaded inverter Eq. (9):

$$\begin{aligned} T_1 &= K_1 + \overline{K_2} * \overline{K_3} \\ T_2 &= \overline{K_1} * K_2 * K_3 \\ T_6 &= K_1 * K_2 * K_3 \\ T_7 &= \overline{K_1} + \overline{K_2} * K_3 \end{aligned} \quad (9)$$

For the NPC inverter Eq. (10):

$$\begin{aligned} T_1 &= \overline{K_1} * K_2 * K_3 + \overline{K_1} * \overline{K_2} * K_3 \\ T_2 &= K_3 + \overline{K_1} * K_2 + K_1 * \overline{K_2} \\ T_6 &= K_1 \\ T_7 &= \overline{K_1} \end{aligned} \quad (10)$$

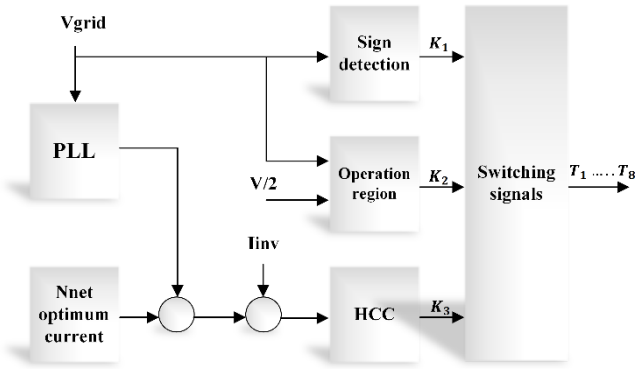

Fig. 8. Control blocks of the inverter.

The control algorithm was implemented in a DSP microcontroller dsPIC 30F4011. It is composed of three interrupt routines with priority. The first interrupt routine is employed to detect the zero crossing of the grid utility to synchronize the inverter with the grid; this interrupt has the highest priority. The second interrupt allows creating of the switching pulses for the inverter power switches and it is generated by the inner timer overflow. To generate a sinusoidal optimal reference current, a unity sinusoidal waveform was discretized into 256 values and stored in the EEPROM of the microcontroller. The maximum power point tracker algorithm calculates the optimal current I_{opt}. This current I_{opt} is multiplied by the unity sinusoidal waveform to have a sinusoidal reference. This reference is compared with the measured inverter output current. Then the difference between them (the error) is compared with the hysteresis band to generate the signal K_3. This control scheme is adopted for the two multilevel inverter topologies.

4. Simulation Validation

To verify the proposed control strategies and the whole system operation, simulation studies were conducted using MATLAB/Simulink. Fig. 9 and fig. 10, represents the results of the NPC multilevel inverter and the cascaded inverter respectively. The top curve represents the grid synchronization signal. The inverter output current and voltage are respectively presented. The inverter current is sinusoidal, and the voltage is composed of 5 levels which confirm the previous analysis. VHB control gives a smooth current shape with low total harmonic distortion (THD=2.62; 2.24 %) for both topologies, compared to the FHB current control. However, the variable band technique increases switching losses due to the increasing of switching frequency. The more the hysteresis band is narrow the more the switching frequency is high. Both inverter topologies give good performance with lower THD (THD < 5 %) as required by inverters connection standards, and the inverter output waveforms are well synchronized with the grid.

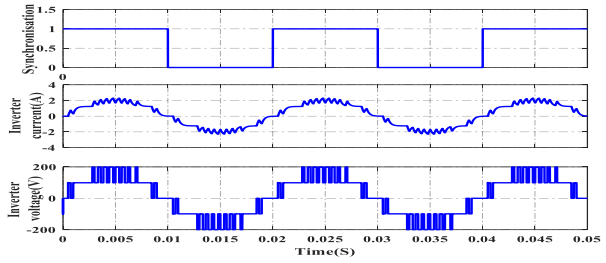

(a) Fixed band 0.3 A

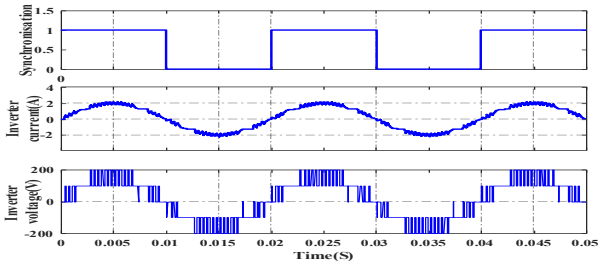

(a) Fixed band 0.3 A

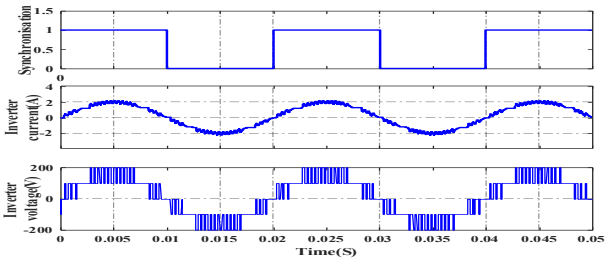

(b) Fixed band 0.2 A

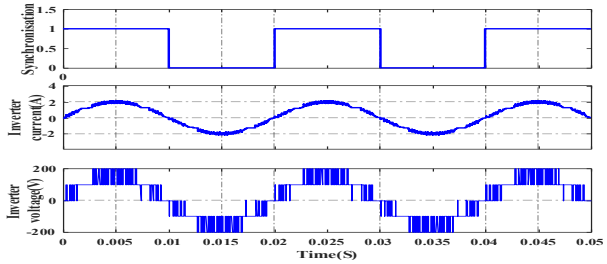

(b) Fixed band 0.2 A

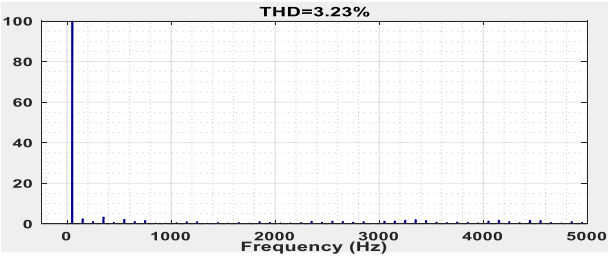

(c) Output current spectrum (band=0.2 A)

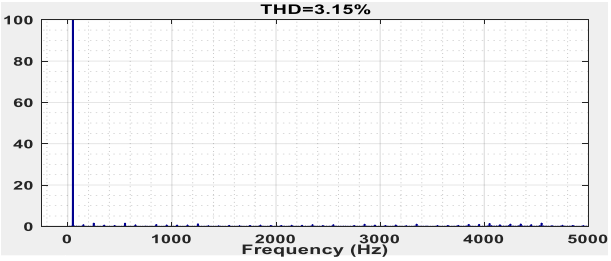

(c) Output current spectrum (band=0.2 A)

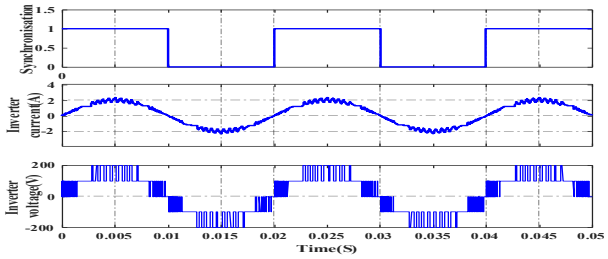

(d) Variable band 0.3 A

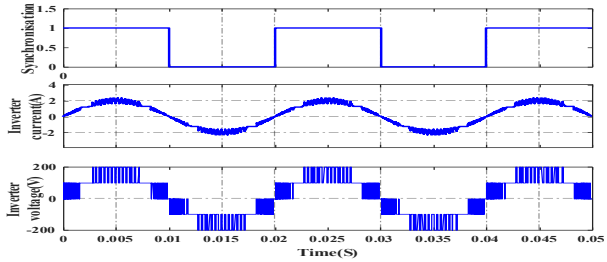

(d) Variable band 0.3 A

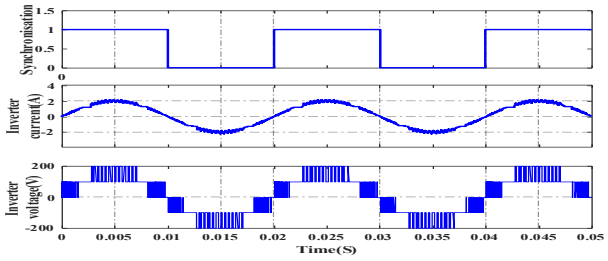

(e) Variable band 0.2 A

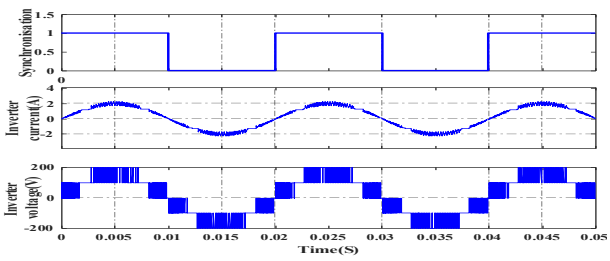

(e) Variable band 0.2 A

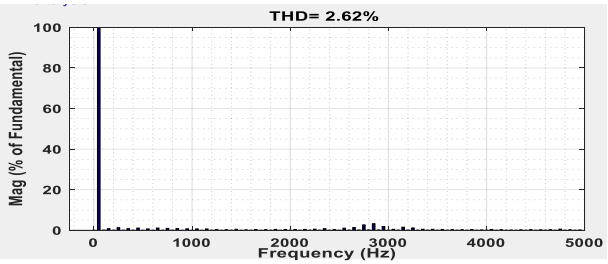

(f) Output current spectrum (band=0.2 A)

Fig. 9. Simulation results of NPC inverter output current (2 A/div), output voltage (200 V/div) and spectrum of the output current.

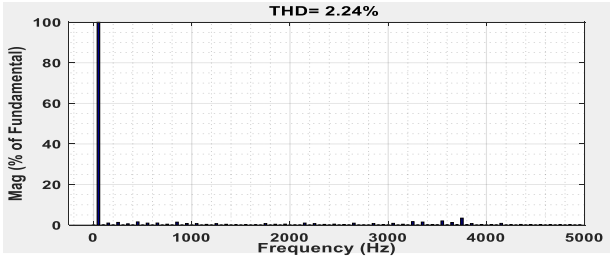

(f) Output current spectrum (band=0.2 A)

Fig. 10. Simulation results of cascaded inverter, output current (2 A/div), output voltage (200 V/div) and spectrum of the output current.

5. Experimental Validation

In order to verify the performance of the developed control algorithms and to validate obtained simulation results, an experimental prototype of both inverters has been built. The control algorithms were implemented in dsPIC microcontroller. Table 4 shows the parameters used for testing. The sampling frequency (S.F) is 15 kHz.

The obtained experimental results are closer to the simulation results. The experimental results with fixed hysteresis are presented in fig.11. Results for the NCP inverter are presented in fig.11 a and results of the cascaded H-bridge (CHB) inverter are in fig. 11 b. All results include the PLL synchronization (first curve), the inverter output current and voltage waveforms respectively. A digital spectrum analyzer was used to compute FFT. The total harmonic distortion (THD) of the output current is presented in Table 5 and Table 6.

For the fixed hysteresis band (fig. 11), the THD is 3.31 % for the NPC inverter and 3.26 % for cascaded inverter (Table 5). For both inverters, the values agree with the standards (<5 %).

For the variable hysteresis band (fig. 12), the current is smoother than the fixed band that can be verified by the measured THD. For the NPC inverter THD=2.75 % and for the cascaded inverter THD=2.35 % (Table 6).

A comparison between obtained THD of both inverters is presented in Table 7.

Table 4. Parameters used for the experimental setup.

P (W)	f (Hz)	V_{grid}	V_{dc}	L(mH)	S.F (kHz)
800	50	220	200	2	15

Table 5. THD values for fixed hysteresis band.

Inverter Topology	Hysteresis band (A)	THD (%)
CHB	0.3	3.26
NPC	0.3	3.31

Table 6. THD values for variable hysteresis band.

Inverter Topology	Hysteresis band (A)	THD (%)
CHB	0.3	2.35
NPC	0.3	2.75

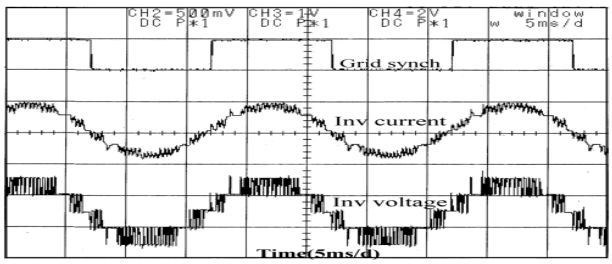

(a)

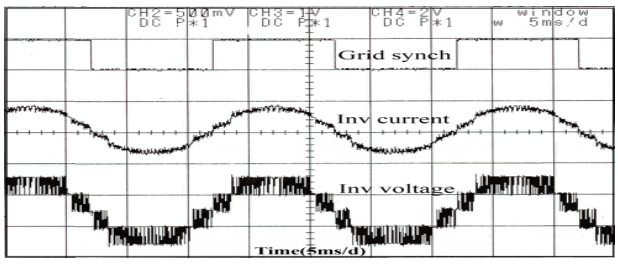

(c)

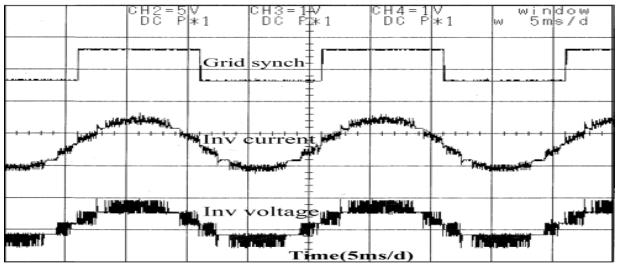

(b)

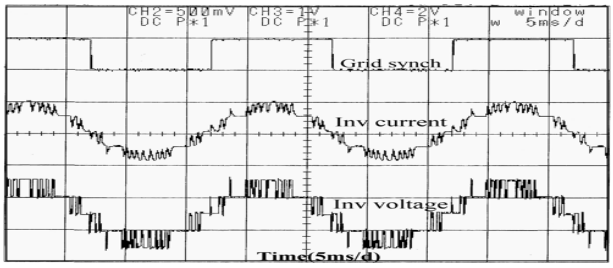

(d)

Fig. 11. Experimental results of fixed hysteresis band, a,b band=0.2 A, c,d band=0.3 A, first curve grid synchronization, second curve output current (2 A/div), third curve voltage (200V/div)

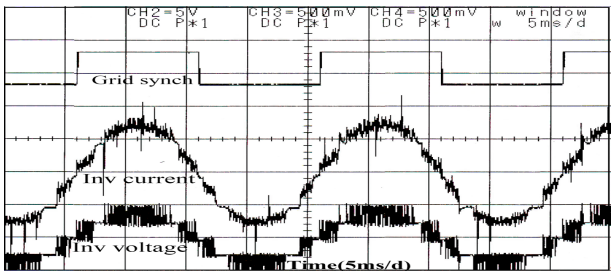

(a)

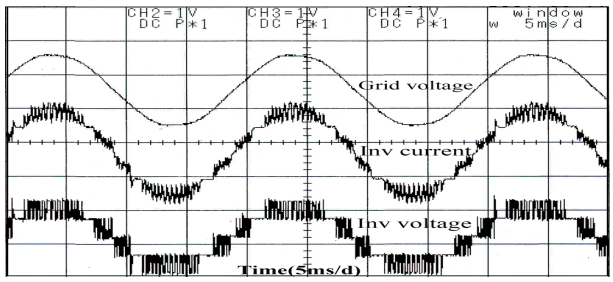

(c)

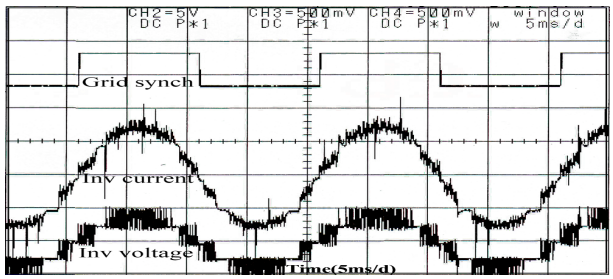

(b)

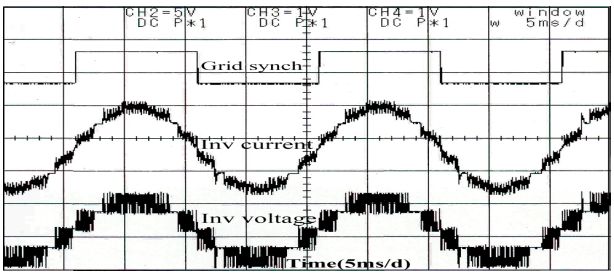

(d)

Fig. 12. Experimental results of variable hysteresis band, a,b band=0.3 A, c,d band=0.2 A, first curve grid synchronization, second curve output current (2 A/div), third curve output voltage (200 V/div)

Other tests were performed to verify the grid synchronization, fault detection and MPPT algorithm robustness when weather conditions change. Results are shown in figure 13. Figures 13 a and b present the synchronization with utility. The inverter output voltage and grid voltage are well synchronized. Figures 13 c and d show islanding tests for utility grid disconnection. Figures 13 e and f show the cases of utility over voltage, under voltage, over frequency and under frequency. The inverters stop their operation in the next cycle for both tests which confirm and satisfy the utility grid-connection criteria.

Table 7. THD values comparison of both inverters.

Hysteresis technique	THD (%) NPC	THD (%) CHB
Fixed band	3.26	3.31
Variable band	2.35	2.75

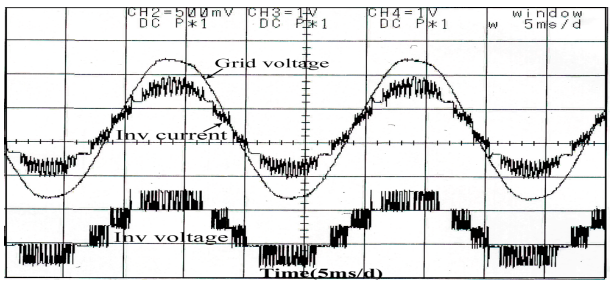

(a)

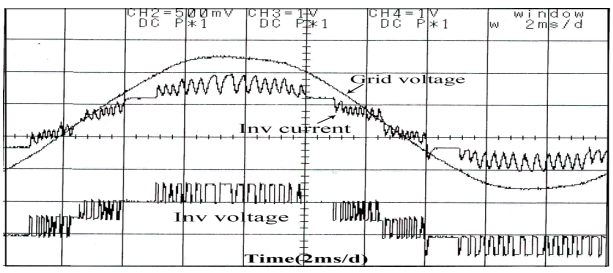

(b)

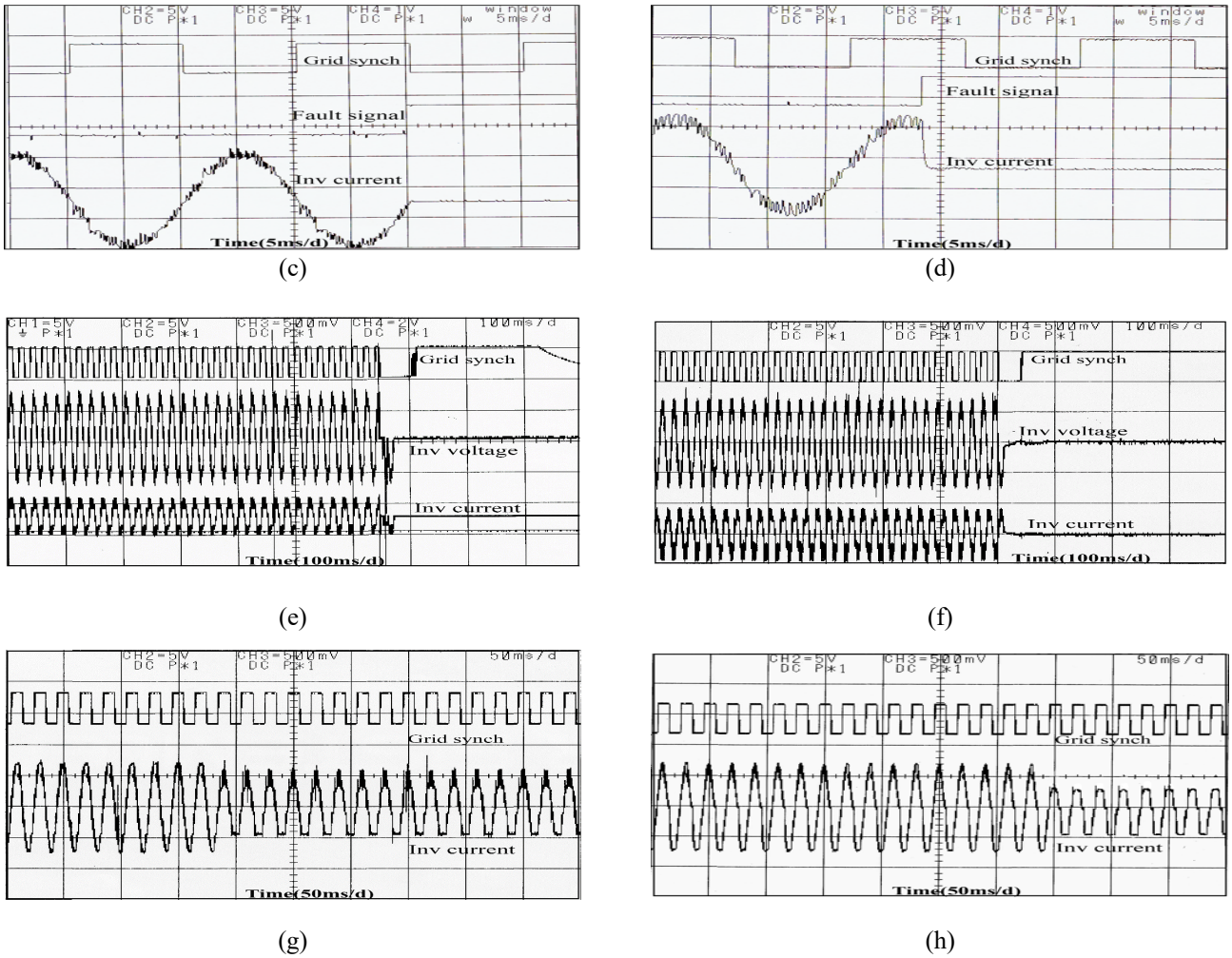

Fig. 13. Results for synchronization, islanding and irradiation change tests, for both inverter topologies.

Figures 13 g and h present performance tests of maximum power tracking by the neural network algorithm for both inverter topologies when solar irradiation change occurs. The inverter's output current follows these changes quickly. This confirms the robustness of the proposed control approaches.

To calculate inverter power losses, MOSFET characteristics from datasheet can be used. In this work we used the IRFP450 MOSFET from International Rectifier. The MOSFET power losses (P_m) is equal to the summation of the conduction losses (P_c) and the switching losses (P_{sw}).

$$P_l = P_c + P_{sw} \tag{11}$$

Based on the datasheet parameters, conduction power losses can be calculated using equation 12 [30],

$$P_c = I_d^2 * R_{ds} * D \tag{12}$$

Where I_d is the RMS current value multiplied by the duty cycle D and R_{ds} is the resistance between the drain and the source when the MOSFET is on. Switching power losses are calculated using equation 13.

$$P_{sw} = \frac{1}{2} * I_d * V_{dd} * F_{sw} * (T_{ri} + T_{fv} + T_{rv} + T_{fi}) \tag{13}$$

where V_{dd} is the input voltage, F_{sw} is the switching frequency, T_{ri}, T_{fi} are respectively the rising and the falling times of the current and T_{rv}, T_{fv} are respectively the raising and the falling times of the voltage.

Table 8 summarizes the power losses of both inverters using the two hysteresis techniques.
The CHB has a higher power losses because it contains more power MOSFETS than NPC inverter especially when the hysteresis variable band technique was used.

Table 8. Power losses of both inverters.

Hysteresis technique	Power losses (W)	
	N.P.C	CHB
Fixed band	21.9	29.2
Variable band	24.2	32.2

6. Conclusion

In this paper performance analysis of grid connected photovoltaic system using two multilevel inverter topologies has been performed. The MPPT controller is implemented using a neural network algorithm to maximize the output power of the PV systems according to environmental

conditions variations. A hysteresis current controller with fixed and variable bands has been used to generate a sine wave signal at the alternating current side of the inverter. This control method allows to track the optimal current delivered by the NNET algorithm. The MPPT algorithm was tested during a day. Other tests were performed to verify the robustness of the developed MPPT algorithm when irradiation changes occur. All control algorithms were implemented in a dsPIC microcontroller, with an interrupt-scheduled algorithm.

The obtained results demonstrate the feasibility and the effectiveness of the proposed prototypes and developed algorithms. The proposed control strategy based on hysteresis, has given good results with low THD and grid synchronization capabilities. The width of the hysteresis band has a very important effect on the inverter output power. The more the hysteresis band is reduced more the power quality is better. Moreover, the VHB controller gives lower current THD but increases switching frequency, this can increase the switching losses. Both of the investigated inverter topologies gave good results. The cascaded inverter gives a lower current THD compared to the NPC topology and it has the advantage of modularity, but it is more expensive due to the amount of power switching transistors it requires.

References

[1] Yahui W, Yong L, Yijia C, Yi T, Li H, Jiye H, "Hybrid AC/DC microgrid architecture with comprehensive control strategy for energy management of smart buildings", Electrical Power and Energy Systems, vol 101, pp. 151–161, 2018.

[2] X. Xu, J. Chen, S. Li, K. Hu and L. Yu, "FPGA Implementation of CPS-SPWM for Grid Connected Photovoltaic System", Asia-Pacific Power and Energy Engineering Conference, Wuhan, pp. 1-4, 2011.

[3] H. Athari, M. Niroomand, M. Ataei, "Review and Classification of Control Systems in Grid-tied Inverters", Renewable and Sustainable Energy Reviews, vol 72, pp. 1167–1176, 2017.

[4] E. Kandemir, N. S. Cetinb, S. Borekci, "A comprehensive overview of maximum power extraction methods for PV systems", Renewable and Sustainable Energy Reviews, vol 78, pp. 93–112, 2017.

[5] B. Xiao, L. Hang, J. Mei, C. Riley, L. Tolbert, and B. Ozpineci, "Modular cascaded H-bridge multilevel PV inverter with distributed MPPT for grid connected applications", IEEE Transactions on Industrial Electronics, vol 51, pp. 1722 – 1731,2014.

[6] C. D. Fuentes, C. A. Rojas, H. Renaudineau, S. Kouro, M. A. Perez, and T. Meynard, "Experimental validation of a single DC bus cascaded H-bridge multilevel inverter for multistring photovoltaic systems", IEEE Transactions on Industrial Electronics, vol 61, pp. 930-934, 2017.

[7] A. Ali ; A. N Hasan ; T. Marwala "Perturb and observe based on fuzzy logic controller maximum power point tracking (MPPT) ", International Conference on Renewable Energy Research and Application (ICRERA), pp. 406–411, 2014.

[8] N. Priyadarshi, A. K. Sharma, S. Priyam, "Practical Realization of an Improved Photovoltaic Grid Integration with MPPT", International Journal of Renewable Energy Research (IJRER), Vol.7, No.4, pp.1880–1891, 2017.

[9] Y. Soufi, M. Bechouat, S. Kahla, K. Bouallegue, "Maximum power point tracking using fuzzy logic control for photovoltaic system", 3rd International Conference on Renewable Energy Research and Applications (ICRERA) Milwaukee, USA 19-22, pp. 902–906, 2014.

[10] S. Saravanan, Ramesh Babu N. "RBFN based MPPT algorithm for PV system with high step up converter", Energy Conversion and Management, vol 122, pp. 239–251, 2016.

[11] M. Hossein M, Hamid Reza Mohammadi, M. Rahimi, "A review on modeling and control of grid-connected photovoltaic inverters with LCL filter", Renewable and Sustainable Energy Reviews, vol 81, pp. 563–578, 2018.

[12] T. T. Tran and M. K. Nguye, "Cascaded five-level quasi-switched-boost inverter for single-phase grid-connected syste", IET Power Electronics, vol 81, pp. 1896-1903, 2017.

[13] Hossein I.E, Sarath B. Tennakoon, "Investigation of a cascaded H-bridge photovoltaic inverter under nonuniform insolation conditions by hardware-in-the-loop test", Electrical Power and Energy Systems, pp 330–340, 2019.

[14] J. Chhor , C. Sourkounis, "Performance evaluation of hysteresis-based PI state control for grid-connected NPC voltage-fed power converter with LCL filter" IEEE 6th International Conference on Renewable Energy Research and Applications (ICRERA), pp. 181-188, 2017.

[15] F. Zare, and G. Ledwich, "A Hysteresis Current Control for Single-Phase Multilevel Voltage Source Inverters: PLD Implementation", IEEE transactions on power electronics, vol 17: pp. 731-738, 2002.

[16] S. Jain, V. Sonti, "A Highly Efficient and Reliable Inverter Configuration Based Cascaded Multilevel Inverter for PV Systems", IEEE transactions on industrial electronics, vol 64, pp. 2865-2875, 2017.

[17] Q-C. Zhong, T. Hornik, "Cascaded Current–Voltage Control to Improve the Power Quality for a Grid-Connected Inverter With a Local Load", IEEE transactions on industrial electronics, vol, 60, 1344-1355, 2013.

[18] Yahya N, Seyed H.H, Saeid G.Z, Behnam M.I, Mehdi S, Josep M.G, "An optimized direct control method applied to multilevel inverter for microgrid power quality enhancement", Electrical Power and Energy Systems, vol 107, pp. 496–506, 2019.

[19] Y. Zhang and C. Qu, "Direct power control of a pulse width modulation rectifier using space vector modulation under unbalanced grid voltages", IEEE transactions on industrial electronics, vol 30, pp. 5892-5901, 2015.

[20] A. Awasthi, D. Patel, "Implementation of Adaptive Hysteresis Current Control Technique for Shunt Active Power Conditioner and Its Comparison with Conventional Hysteresis Current Control Technique", IEEE International Conference on Signal Processing, Informatics, Communication and Energy Systems (SPICES), Kollam, pp.1-6, 2017.

[21] Shriram S. Rangarajan ; E. Randolph Collins ; J. Curtiss Fox, "Comparative impact assessment of filter elements associated with PWM and hysteresis controlled PV on network harmonic resonance in distribution systems", 2017 IEEE 6th International Conference on Renewable Energy Research and Applications (ICRERA), pp. 80-85, 2017.

[22] R. Patjoshi, K. Mahapatra, "Resistive optimization with enhanced PLL based nonlinear variable gain fuzzy hysteresis control strategy for unified power quality conditioner", Electrical Power and Energy Systems, vol, 83, pp. 352–363, 2016.

[23] R. Bakhshi, J. Sadeh, "Voltage positive feedback based active method for islanding detection of photovoltaic system with string inverter using sliding mode controller", Solar Energy, vol 137, pp. 564–577, 2016.

[24] M. Robitaille, K. Agbossou, M. L. Doumbia, R. Simard, "slanding Detection Method for a Hybrid Renewable Energy System", International Journal of Renewable Energy Research (IJRER), Vol.1 , No.1, pp.41-53, 2011.

[25] Ch. Rami Reddy, K. Harinadha Redd, "Islanding Detection Techniques for Grid Integrated DG –A Review", International Journal of Renewable Energy Research (IJRER), Vol 9, No 2, pp. 960–977, 2019.

[26] ESRAM, Trishan, CHAPMAN, Patrick L, "Comparison of photovoltaic array maximum power point tracking techniques", IEEE Transactions on energy conversion, vol 22, pp. 439-449, 2017.

[27] Mohamed DELLA KRACHAI, Abdelhamid MIDOUN, "High efficiency maximum power point tracking control in photovoltaic-grid connected plants", Faculty of Electrical Engineering and Informatics, Technical University of Košice, Slovak Republic, pp. 1335-8243, 2007.

[28] K. Amara, A. Fekik, D. Hocine, M. L. Bakir, E.B. Bourennane, T. Ali Malek, A. Malek, "Improved Performance of a PV Solar Panel with Adaptive Neuro Fuzzy Inference System ANFIS based MPPT" 7th International Conference on Renewable Energy Research and Applications (ICRERA), pp. 1098-1101. 2018.

[29] E. B.-R. Lin and D.-J. Chen, "Single-phase neutral point clamped AC/DC converter with the function of power factor corrector and active filter", IEE Proc.-Electr. Power, vol 149, pp. 19-30, 2002.

[30] INFINEON Application Note, MOSFET Power Losses Calculation Using the Data Sheet Parameters, Automotive Power, V 1.1, July 2006.